Supporting Information

Toward Rechargeable Persistent Luminescence for the First and Third Biological Windows via Persistent Energy Transfer and Electron Trap Redistribution

Jian Xu,*[,†] Daisuke Murata,[†] Jumpei Ueda,[†] Bruno Viana,[‡,§] and Setsuhisa Tanabe[†]

[†]Graduate School of Human and Environmental Studies, Kyoto University, Kyoto 606-8501, Japan

[‡]PSL Research University, Chimie ParisTech-CNRS, Institutde Recherche de Chimie Paris, Paris 75005, France

[§]Chimie ParisTech-CNRS, Paris cedex F-75231, France

[*]E-mail: xu.jian.57z@st.kyoto-u.ac.jp

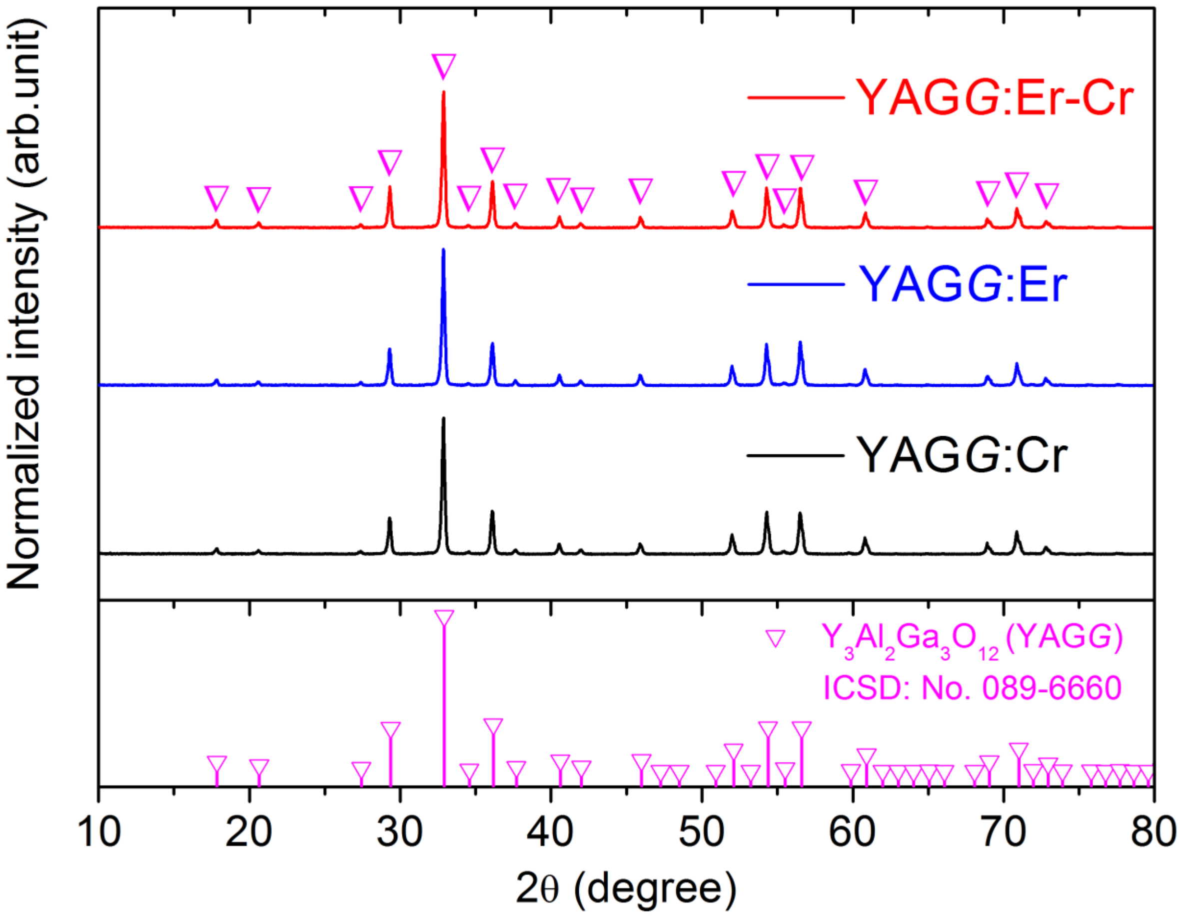

Figure S1. X-ray diffraction (XRD) patterns of the YAG*G*:Cr, YAG*G*:Er, YAG*G*:Er-Cr garnet ceramic samples

Phase crystallization of the YAG*G*:Cr, YAG*G*:Er and YAG*G*:Er-Cr garnet ceramic samples were identified by X-ray diffraction (XRD) measurements (Ultima Ⅳ, Rigaku), utilizing nickel filtered Cu Kα_1 radiation (1.5406 Å). All of the prepared samples are confirmed to be single phases matching well with the standard card (ICSD: No. 089-6660) of $Y_3Al_2Ga_3O_{12}$ (YAG*G*).

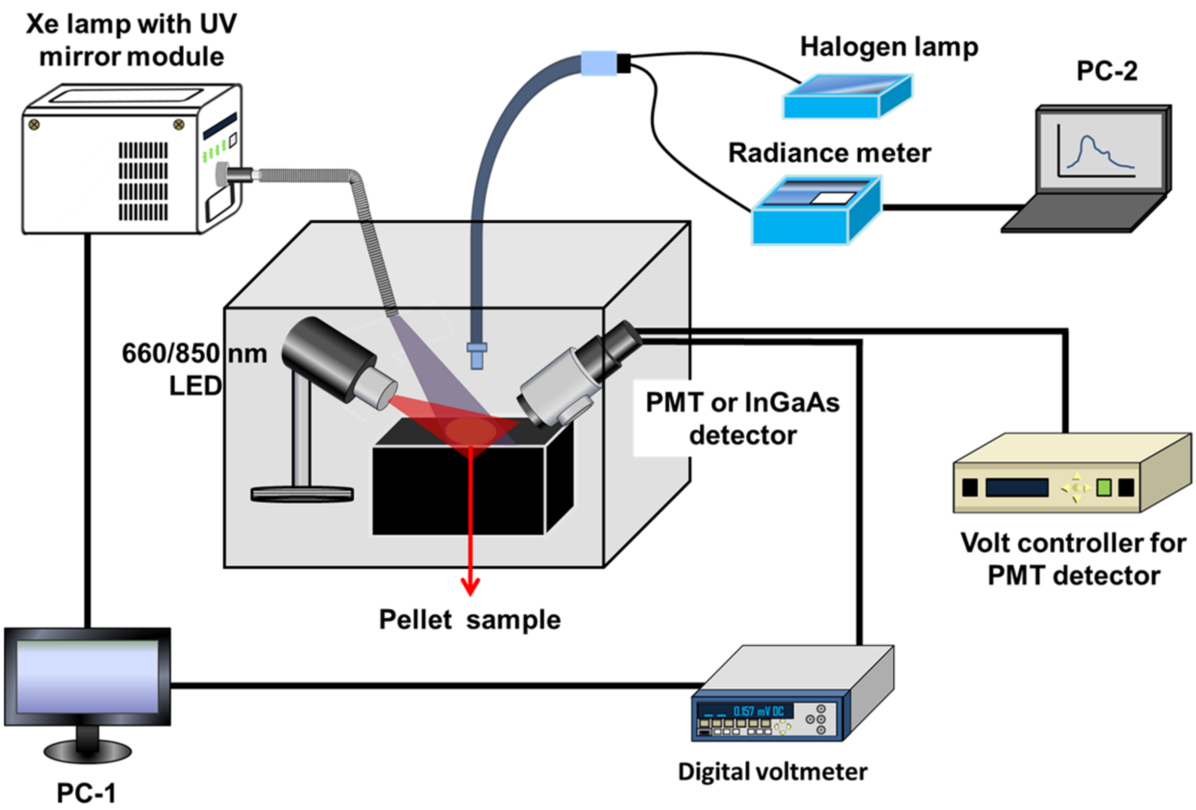

Figure S2. The measurement setup of persistent luminescent and photostimulation induced persistent luminescent decay curves

The persistent luminescent decay curve of the YAG*G*:Er-Cr sample after being excited for 5 min by a 300 W Xe lamp (MAX-302, Asahi Spectra) with a UV (250-380 nm) mirror module was measured at 25 ℃ using a PMT (R11041, Hamamatsu Photonics) detector or an InGaAs photodiode detector (IGA-030-H, Electro-Optical System Inc.,). In order to monitor the Cr^{3+} emission, the PMT detector was covered with 580 nm short-cut and 750 nm long-cut filters to filter out all but the Cr^{3+} luminescence. In order to monitor the Er^{3+} luminescence, the InGaAs photodiode detector was covered with a 1450 nm short-cut filter to filter out all but the Er^{3+} luminescence, then the decay curves were calibrated into the absolute radiance (in unit of $mW{\cdot}sr^{-1}{\cdot}m^{-2}$) using a radiance measurement setup (BW-L1, Konica-Minolta) comprising a CCD spectrometer (Glacier X, B&W Tek Inc), a fiber, and a collimator lens. Photostimulation was induced by a 660 nm red LED (LED660/L-STND, Optocode) with a power density of ~0.14 W/cm^2 and full width at half maximum (FWHM) of 20 nm or an 850 nm LED (LED850/L-STND, Optocode) with a power density of ~0.14 W/cm^2 and FWHM of 48 nm.

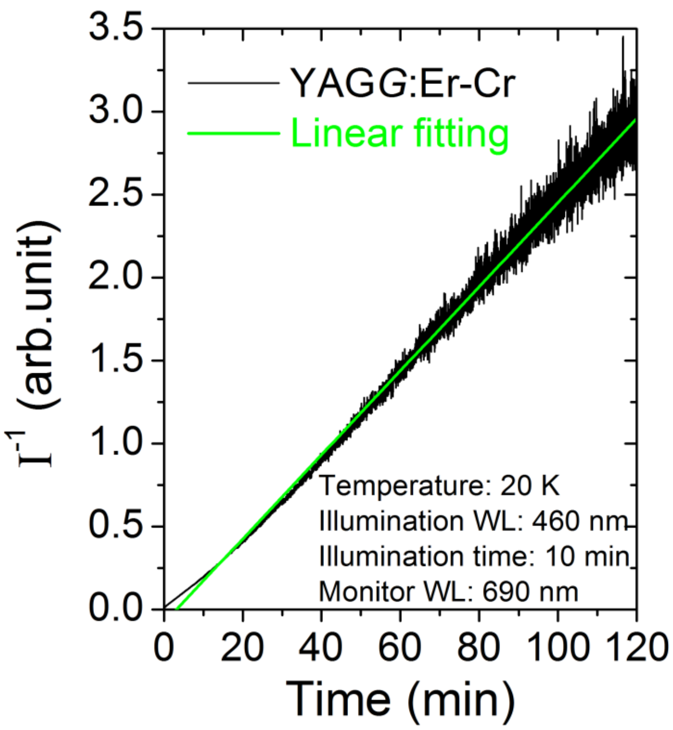

Figure S3. Low-temperature persistent luminescent decay curve of the YAG*G*:Er-Cr ceramic sample monitoring Cr^{3+} emission at 20 K after ceasing 460 nm excitation for 10 min

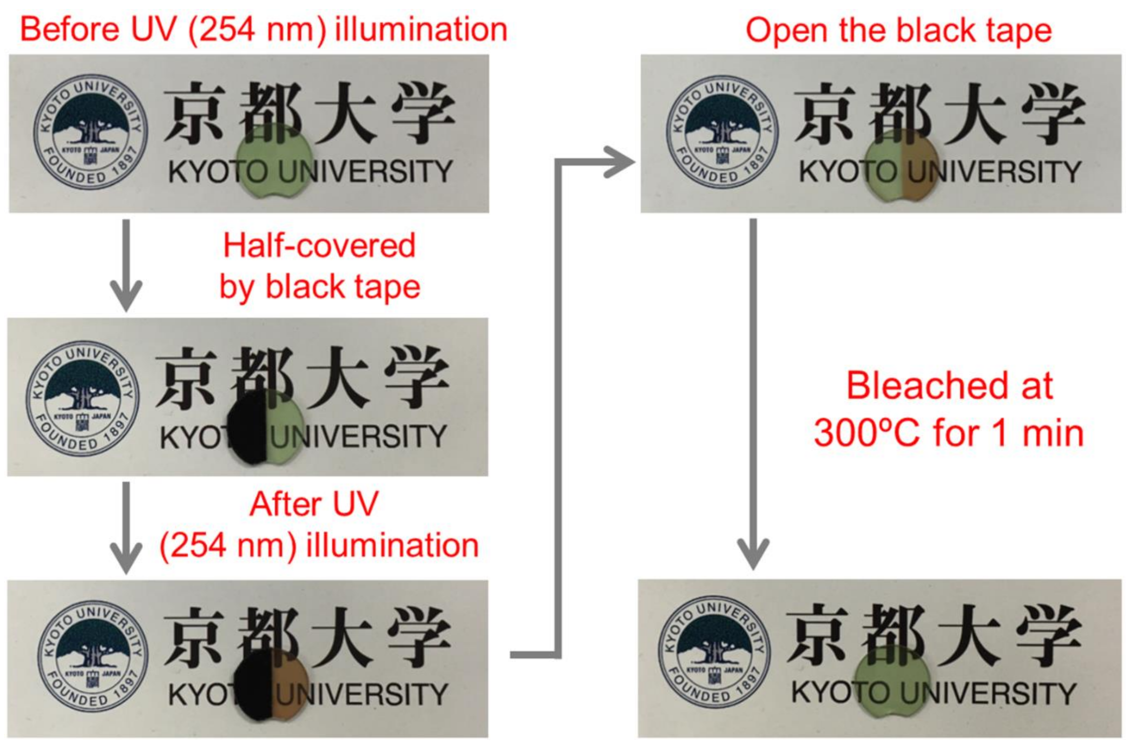

Figure S4. Photochromic phenomenon of the YAG*G*:Er-Cr transparent ceramic (thickness of 1 mm) after UV (254 nm) illumination for 1 min

Although compared with the UV light, the charging efficiency of visible light (*e.g.*, 460 nm blue light) is much lower, the YAG*G*:Er-Cr persistent phosphor still exhibits the PersL behavior even at 20 K with a very low thermal assisted energy (**Figure S3**), which suggests that a trapping-detrapping tunneling process independent of temperature occurs in the forbidden band between the intrinsic-defect-related electron trap and the Cr^{3+}: $^4T_1$ (^4F) level. On the other hand, the intrinsic defects [color centers, either F^+ centers or oxygen vacancies ($V_O^{\bullet\bullet}$ or $V_O^{\bullet}$) as electron traps] cause a significant photochromic phenomenon in YAG*G*:Er-Cr under ambient conditions (taking a transparent ceramic sample with the same composition as a vivid example in **Figure S4**). The body color of the YAG*G*:Er-Cr transparent ceramic changes from green to brown under UV (254 nm) charging for 1 min, and it takes several days to gradually or a short time under thermal bleaching at a relatively high temperature (*e.g.*, 300 ℃ for 1 min) to return back its original green body color, which suggests that photochromic centers due to intrinsic defects in YAG*G* host can serve as the deep electron trap (Trap-II). Furthermore, the coloration and decoloration processes in this material can repeatedly occur upon UV charging and thermal bleaching for many times, respectively.

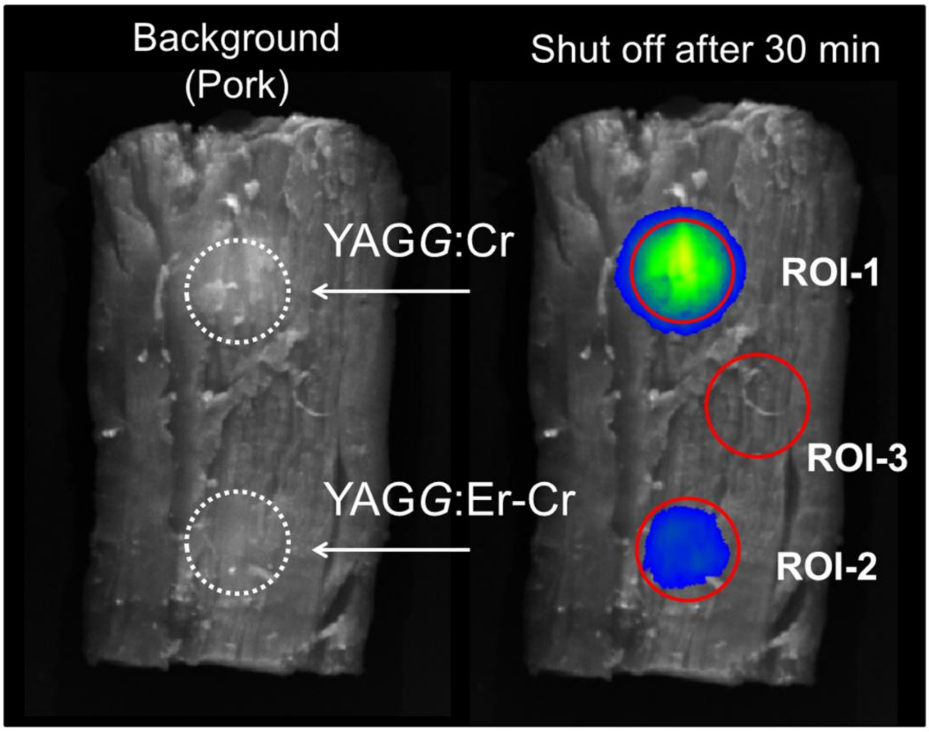

Figure S5. Calculation of signal-to-noise ratio (SNR) from persistent luminescence images through raw-pork tissues (thickness of 1 cm) monitoring Cr^{3+} emission of the YAG*G*:Cr and YAG*G*:Er-Cr ceramic pellets by Si CCD camera after a mercury lamp (254 nm, 6 W output) illumination for 10 min

Composition/Background	Region of Interest (ROI)	Signal-to-Noise Ratio (SNR)
YAG*G*:Cr (ROI-1)	$9.89 \pm (0.19) \times 10^3$	~157
YAG*G*:Er-Cr (ROI-2)	$7.67 \pm (0.15) \times 10^3$	~121
Pork (ROI-3)	$0.63 \pm (0.07) \times 10^2$	-

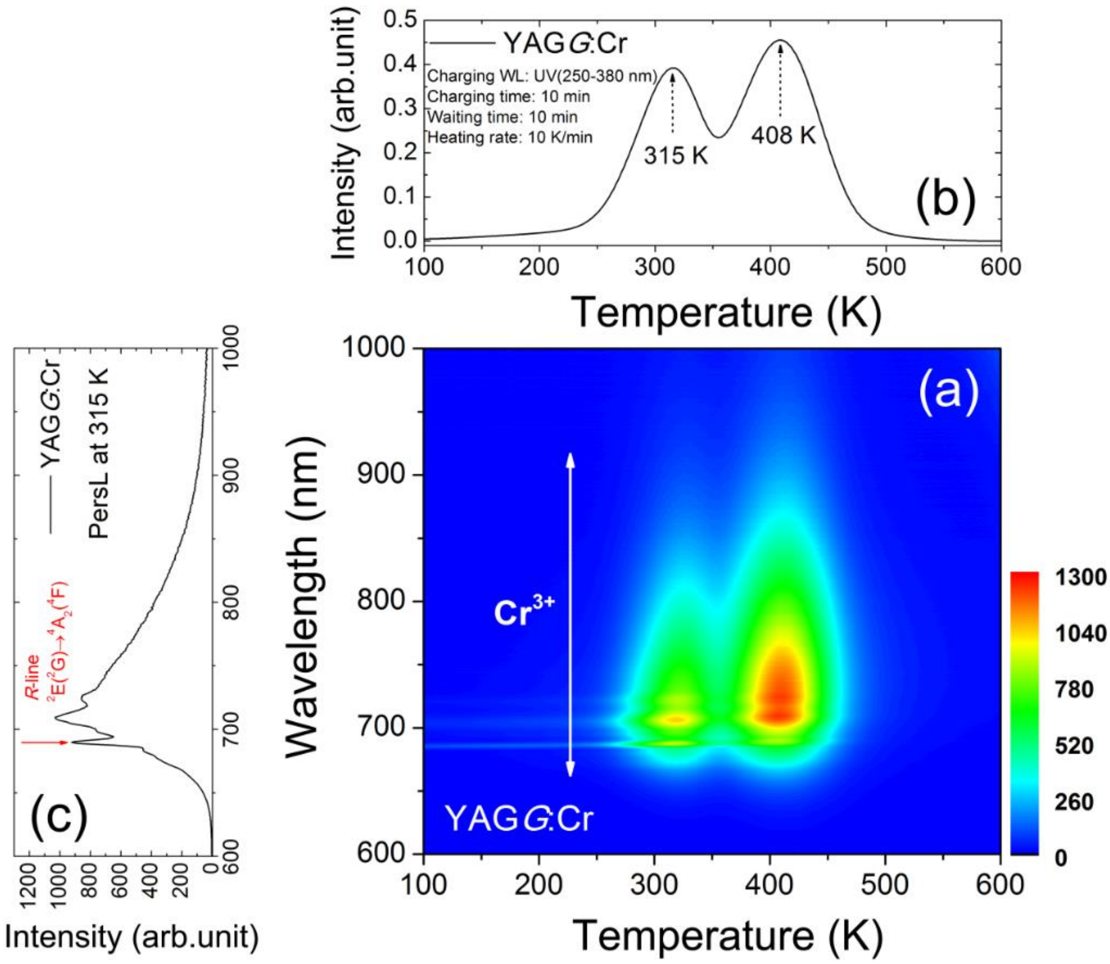

Figure S6. (a) Wavelength-temperature (λ-T) contour plot of the YAG*G*:Cr sample (b) thermoluminescence (TL) glow curve and (c) TL emission spectrum at 315 K

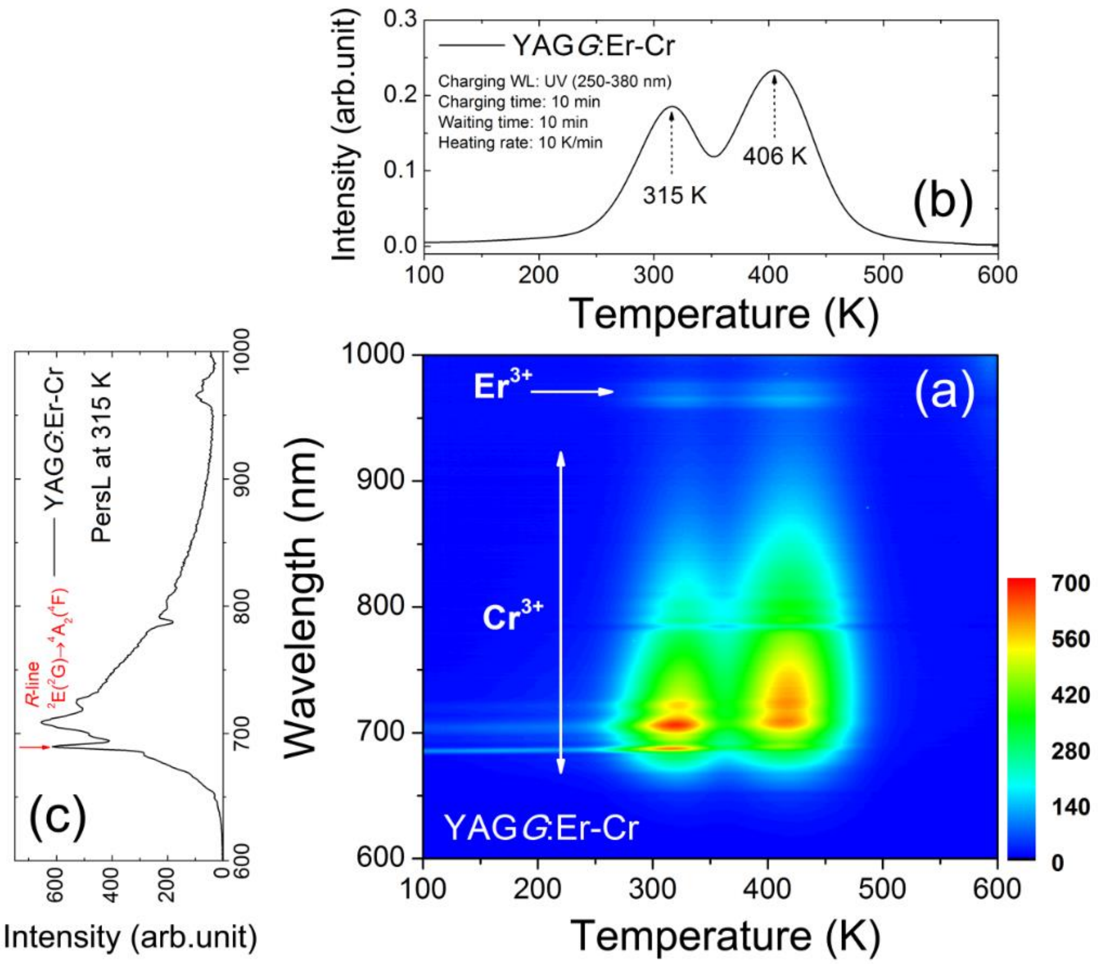

Figure S7. (a) Wavelength-temperature (λ-T) contour plot of the YAG*G*:Er-Cr sample (b) thermoluminescence (TL) glow curve and (c) TL emission spectrum at 315 K

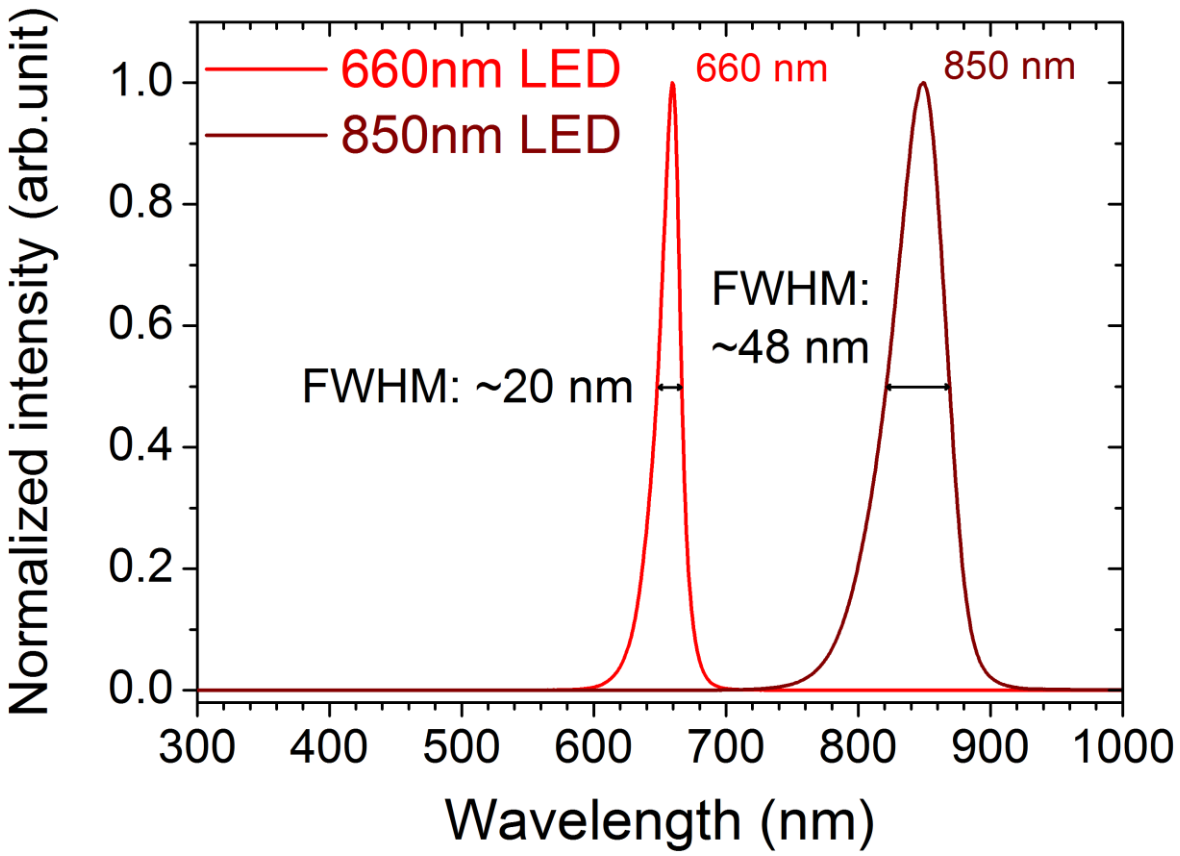

Figure S8. The normalized emission spectra of the 660 nm LED (LED660/L-STND, Optocode) with a power density of ~0.14 W/cm^2 and FWHM of 20 nm as well as the 850 nm LED (LED850/L-STND, Optocode) with a power density of ~0.14 W/cm^2 and FWHM of 48 nm

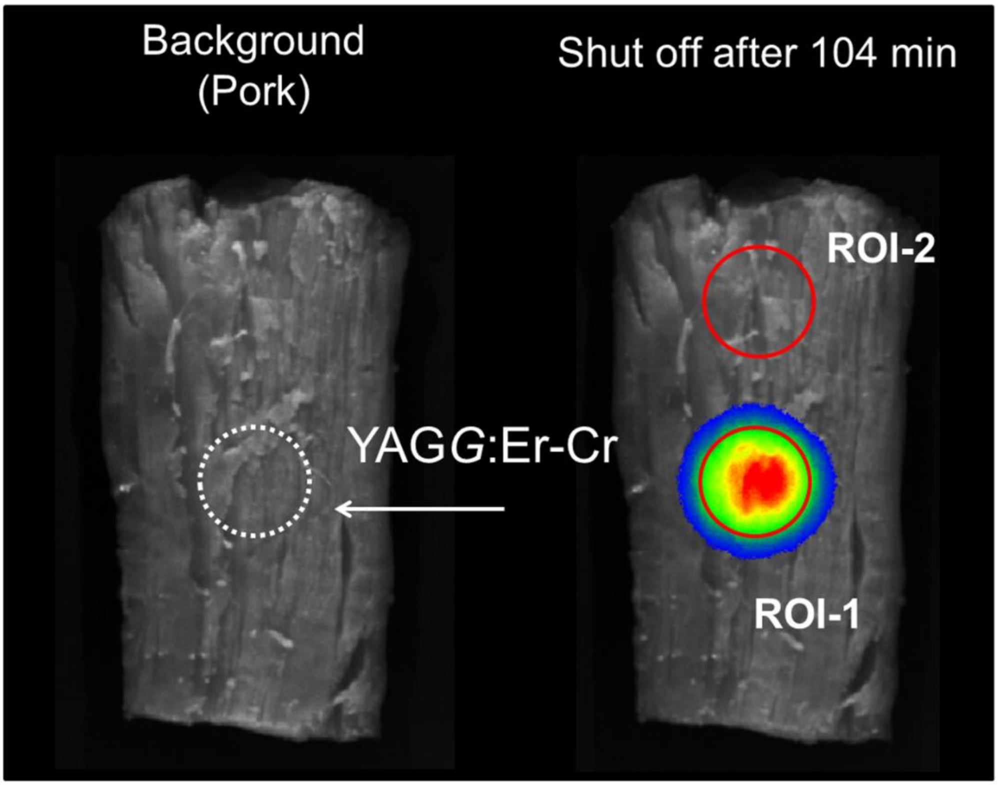

Figure S9. Calculation of signal-to-noise ratio (SNR) from persistent luminescence images through raw-pork tissues (thickness of 1 cm) monitoring Cr^{3+} emission of the YAG*G*:Er-Cr ceramic pellet by Si CCD camera after a mercury lamp (254 nm, 6 W output) illumination for 10 min and 4-cycle 660 nm LED photostimulation for 1 min with 20 min interval

Composition/Background	Region of Interest (ROI)	Signal-to-Noise Ratio (SNR)
YAG*G*:Er-Cr (ROI-1)	$1.90 \pm (0.58) \times 10^3$	~31
Pork (ROI-2)	$0.62 \pm (0.02) \times 10^2$	-